Advance Publication by J-STAGE

Mechanical Engineering Journal

DOI: 10.1299/mej.24-00129

Received date : 29 March, 2024

Accepted date : 20 June, 2024

J-STAGE Advance Publication date : 30 June, 2024

Effect of artificial defect on tensile properties of thin titanium alloy wire

Junji SAKAMOTO*, Naoya TADA*, Takeshi UEMORI* and Koyo OISHI*
*Okayama University, 3-1-1 Tsushimanaka, Kita- ku, Okayama 700-8530, Japan
E-mail: sakamoto-junji@okayama-u.ac.jp

Abstract
This study investigated the effects of artificial defects, introduced via focused ion beam (FIB) processing, on the tensile properties of thin titanium alloy wires (Ti-6Al-4V). Results indicated that the defective wires fractured when the net-section nominal stress reached the ultimate tensile strength of the smooth wires, probably because of localized stress concentrations relaxing due to plastic deformation around the defects. The effect of defects on tensile properties was classified into three regions based on the size of the defect area. In the case of small defects, wires fractured at the smooth area away from the defects where the cross-sectional strength was lower. In this case, the defects minimally affected the tensile properties. This is attributable to variations in the cross-sectional strength of the wire, which resulted in some sections with lower strength as compared with the defect area. In the case of medium-sized defects, the fracture strain decreased gradually as the defect area increased. Finally, in the case of large defects, the fracture strain was extremely small. The boundary between the medium-sized and large defects indicates the transition from plastic deformation to no plastic deformation in the smooth area.

Keywords : Ti-6Al-4V, Thin wire, Tensile properties, Defect, Focused ion beam, Net-section nominal stress, Fracture surface, Fracture strain

1. Introduction

Ti-6Al-4V is used in the medical field because of its light weight, excellent heat and corrosion resistance, and biocompatibility (Narushima, 2005). In medicine, the demand for miniaturization of various medical devices is increasing because of the increasing drive towards minimally invasive treatments intended to reduce the mental and physical stress of patients. Wires that are small and thin, and yet retain appropriate mechanical properties, are required. Damage to the wire components of miniaturized medical devices may cause significant harm to the human body, and even when thin wires are used in other devices, damage may lead to device failure. In particular, defects on the surfaces of thin wires during manufacturing or service processes can lead to damage and ultimately device failure. Therefore, it is important to evaluate the effects of small surface defects on the mechanical properties of thin Ti-6Al-4V wires to improve the reliability and safety of devices dependent on such wires.

Several studies have been conducted on the tensile properties of Ti-6Al-4V. For example, Horiya et al. (1989) reported that the strength and toughness of Ti-6Al-4V are mainly affected by microstructural factors, especially the microcracks which are initiated near the notch under load, which significantly affect the fracture toughness. Bridier et al. (2005) analyzed slip systems activated by tension in Ti-6Al-4V in relation to local grain orientation. Zhang et al. (2016) performed microscopic experiments and analyses on uniaxial tension in Ti-6Al-4V, analyzing mechanisms and morphology of fracture based on plastic strains in microstructures such as α and β phases. Elambasseril et al. (2019) used CT analysis to reveal the three-dimensional distribution of defects in Ti-6Al-4V created by the additive manufacturing method and discussed their effects on tensile properties. Although the tensile properties and defect effects in bulk Ti-6Al-4V have been investigated, it is understood that these properties might differ between bulk forms and small material forms such as thin wires (e.g., Miyabe et al., 2011; Sakamoto et al., 2023); it remains unclear how defects affect the

tensile properties of thin Ti-6Al-4V wires.

In this study, various defects of differing sizes were introduced into thin Ti-6Al-4V wires using a focused ion beam (FIB) to investigate the effects of the defects on the tensile properties of thin titanium alloy wires.

2. Methods

2.1 Material and tensile test

A thin Ti-6Al-4V wire with a diameter of approximately 0.2 mm manufactured by Tokusen Kogyo Co., Ltd., was used as the specimen. Table 1 lists the chemical composition of Ti-6Al-4V. Figure 1 shows inverse pole figure maps of Ti-6Al-4V. The material featured a fiber texture with an average grain size of 0.8 μm. Because the grain size was sufficiently small compared with the diameter of the specimen, the effect of the local microstructure on the tensile properties likely to be insignificant. Electropolishing was performed under the conditions listed in Table 2 to obtain a smooth specimen surface. The diameters of the electropolished specimens were approximately 0.18 mm. After electropolishing, two copper wires for displacement measurements were bonded to the center of the specimen at a distance of 4 mm. Subsequently, FIB was used to introduce defects with two different shapes, wedge and cylindrical, on the specimen surface between the copper wires (Fig. 2). In this study, the wedge defects were used to induce high stress concentrations, and the cylindrical defects were used to induce low stress concentrations. For wedge defects, several differently sized defects with surface lengths (a), widths (b), and depths (c) of 20:1:8 were employed. For the cylindrical defects, several differently sized defects with a diameter (a) and depth (c) of 5:2 were employed. The FIB processing conditions were determined based on those previously described by the authors (Sakamoto et al., 2018). The specimens with wedge and cylindrical defects were denoted WDSa and CDSa, respectively, based on the surface length and diameter a [μm] of the defects. Smooth specimens were denoted SS. Figure 3 shows a schematic of a specimen. Jigs made of SUS304 stainless steel were glued to both ends of the thin wire 8 mm apart. Cyanoacrylate adhesive was used to bond the jigs. Tensile tests were conducted using an electromagnetic-force micromaterial-testing machine (Shimadzu Corp., MMT-100NB-10) at a displacement rate of 0.001 mm/s until the specimens fractured. After the tensile tests, the specimens were observed by scanning electron microscopy (SEM).

Table 1 Chemical composition of Ti-6Al-4V (wt.%).

C	N	Fe	O	Al	V	Ti
0.01	0.0003	0.2	0.09	6.15	4.09	Bal.

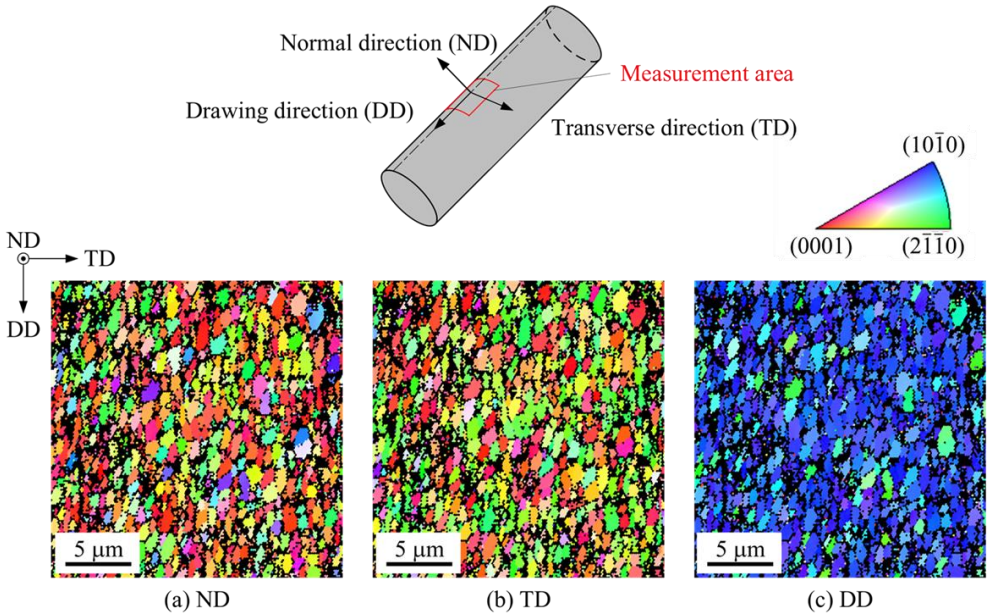

Fig. 1 Inverse pole figure maps of thin titanium alloy wire.

Table 2 Electrolytic polishing conditions.

Solution	Methanol 300 [ml]
	2-butoxyethanol 180 [ml]
	Perchloric acid (70%) 30 [ml]
Cathode	Stainless steel
Anode	Specimen (titanium alloy)
Temperature	218 [K]
Voltage	D.C. 20 [V]
Time	20 [min]

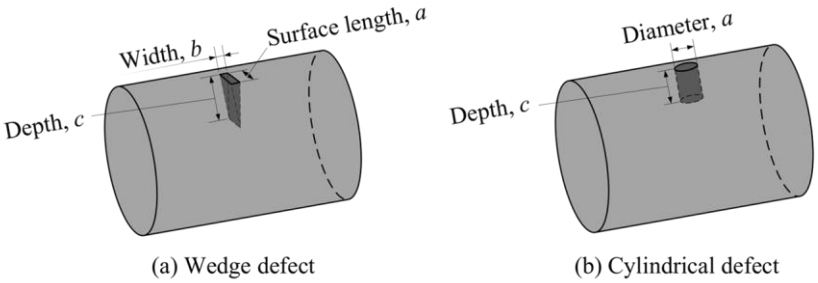

Fig. 2 Shapes and dimensions of artificial defects.

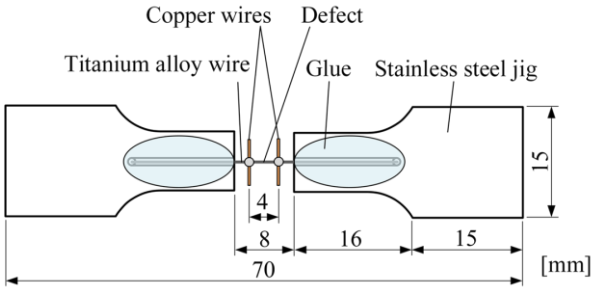

Fig. 3 Shape and dimensions of tensile specimen.

2.2 Parameter calculation method

Several parameters were used to evaluate the tensile properties of the specimens with defects. The calculation methods for these parameters are as follows:

The nominal stress (σ_n) and maximum net section nominal stress ($\sigma_{net,max}$) were calculated. σ_n was calculated by Equation (1) using the average diameter of the smooth part (D) measured based on the scanning ion microscopy (SIM) image of the specimen before the test. σ_n in specimens with defects is the apparent nominal stress, which does not consider the area of the defect. The maximum nominal stress was considered as the tensile strength (σ_B).

$$\sigma_n = \frac{F}{\frac{\pi D^2}{4}} \tag{1}$$

$\sigma_{net,max}$ was calculated using Equation (2). Figure 4 shows a schematic of the parameters used for the calculation of $\sigma_{net,max}$. $\sigma_{net,max}$ is the maximum nominal stress calculated based on the net section area of the defective part before the test (grey area in Fig. 4). F_{max} is the maximum load obtained from the load cell of the testing machine and S_{defect} is the product of the surface length or diameter a calculated from the SIM image and the depth c estimated from the FIB dose. Table 3 lists the diameters, shapes, and sizes of the defects in the specimens used in this study. Because the time required to introduce a defect via FIB processing depends on the volume of the defect, the processing time for a cylindrical defect is much longer than that for a wedge defect. Therefore, large cylindrical defects were not considered in this study.

$$\sigma_{\text{net,max}} = \frac{F_{\max}}{\frac{\pi D^2}{4} - S_{\text{defect}}} \tag{2}$$

The nominal strain (ε_n) was calculated for SS, WDS, and CDS using the distance between the two copper wires measured with a telecentric measurement system (Keyence corp., TM-X5040).

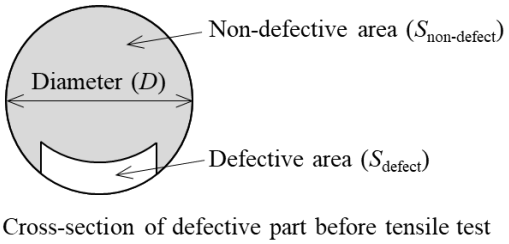

Fig. 4 Schematic illustration of parameters for calculation of $\sigma_{\text{net,max}}$.

Table 3 Diameter of specimens used in this study and the corresponding defect shape and size.

Specimen	Measured diameter of specimen, D [μm]	Defect shape	Defect size	
			Measured surface length or diameter, a [μm]	Estimated depth, c [μm]
SS-1	182	-	-	-
SS-2	197	-	-	-
SS-3	180	-	-	-
WDS25	181	Wedge	24.4	7.50
WDS50	184	Wedge	49.0	15.0
WDS75	183	Wedge	74.5	22.5
WDS100	184	Wedge	98.8	30.0
WDS110	184	Wedge	110	33.0
WDS120	191	Wedge	121	36.0
WDS150	171	Wedge	152	45.0
CDS50	167	Cylindrical	48.9	15.0
CDS75	188	Cylindrical	75.3	22.5

3. Results and discussion

3.1 Stress-strain curves and fracture morphology

Figure 5 shows the relationship between σ_n and ε_n for (a) all specimens and (b) extracted specimens with characteristic behavior. The tensile strength and fracture strain decreased with increasing defect-area size. In the stress-strain diagram, plastic deformation is confirmed after elastic deformation in specimens SS, WDS25, WDS50, WDS75, CDS50, and CDS75, whereas almost no plastic deformation is exhibited in specimens WDS100, WDS110, WDS120, and WDS150. A comparison of WDS50 and WDS75 with CDS50 and CDS75 showed that there was no significant difference due to the defect shape.

The SS specimens were entirely smooth and therefore, their fractures were all in smooth areas. Despite the introduction of defects, the WDS25 and WDS50 specimens also fractured at the smooth (non-defective) areas. The other specimens fractured at the defect sites. Figure 6 shows SEM images of the fracture surfaces of the SS, WDS50, WDS75, and CDS75 specimens after the tensile tests. For the SS and WDS50 specimens, dimples were observed on the fracture surfaces in the smooth areas, indicating a ductile fracture morphology. For the WDS75 and CDS75 specimens, dimples were observed on the fracture surfaces at the defect sites, indicating a ductile fracture morphology, although the reduction in the cross-sectional area was smaller than that of the fracture surface in the smooth area. The other specimens fractured

at defect sites and exhibited the same ductile fracture morphologies. Therefore, for specimens with large defects, no plastic deformation was observed in the apparent stress-strain curves; however, plastic deformation occurred locally at the defect sites.

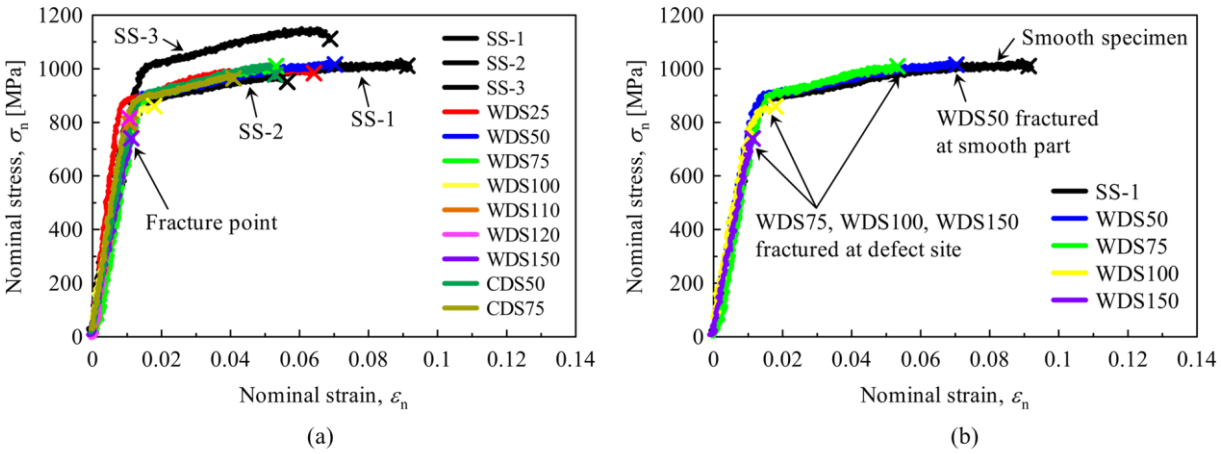

Fig. 5 Relationship between nominal stress and nominal strain for (a) all specimens and (b) extracted specimens with characteristic behavior.

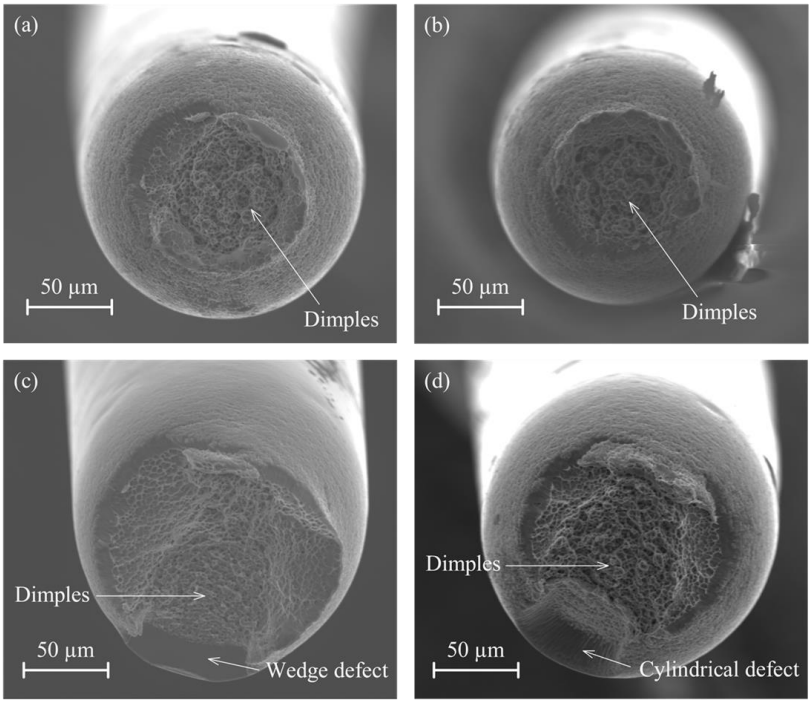

Fig. 6 SEM images of fracture surfaces of (a) SS, (b) WDS50, (c) WDS75, and (d) CDS75.

3.2 Effects of defects on each parameter

Figure 7 shows the relationship between the tensile strength (σ_B) and the ratio of the defective area to the cross-sectional area (S_{defect}/S). When S_{defect}/S was ≤ 0.03, the specimens fractured at the smooth areas and not at the defect sites, and the region that was not affected by the defects was denoted Region I. When S_{defect}/S was > 0.03, the specimens fractured at the defect sites, and σ_B decreased with increasing defect area. There was no significant difference in σ_B between specimens with wedge defects and those with cylindrical defects.

Figure 8 shows the relationship between the fracture strain (ε_f) and S_{defect}/S. S_{defect}/S was classified into three regions according to the tendency of ε_f. Region I was unaffected by the defects described above. In Region II ε_f decreased with increasing defect area, and in Region III ε_f decreased significantly. The boundary between Regions II and III in S_{defect}/S was approximately 0.11. The significance of this value is discussed below.

Figure 9 shows the relationship between $\sigma_{net,max}$ and S_{defect}/S. The values of $\sigma_{net,max}$ for the specimens with defects were almost constant and similar to those for the SS specimens. This suggests that the local stress concentration near the defect has almost no effect on $\sigma_{net,max}$ and that only the reduction in the cross-sectional area due to the defect has an effect on the tensile strength. Takao and Kusukawa (1991) performed fatigue tests using notched specimens of pure titanium and indicated that pure titanium had a lower notch sensitivity than other metallic materials with respect to fatigue crack initiation. They attributed this to the hexagonal-close-packed crystal structure of titanium. In the tensile tests conducted by the authors, in addition to the low notch sensitivity due to the hexagonal-close-packed crystal structure, the local stress concentration in the vicinity of the defect almost disappeared owing to sufficient plastic deformation of the defect area.

Based on the above results, the fracture conditions, fracture positions, and fracture strains of the specimens with defects are discussed. Figure 10 shows schematics of the distributions of tensile strength, 0.2% proof stress, and net-section nominal stress. Figures 10(a), (b), and (c) show specimens with small (Region I: $0 < S_{defect}/S \leq 0.03$), medium-sized (Region II: $0.03 < S_{defect}/S \leq 0.11$), and large (Region III: $0.11 < S_{defect}/S$) defects, respectively. The tensile strength and 0.2% proof stress in the figures are considered to be distributed due to microstructural variations. Conversely, although the distribution of the net-section nominal stress is also attributed to the variation in the cross-sectional area, the variation in stress is < ~1% owing to the variation in diameter, and thus, it is neglected. For all the specimens with defects in this study, the fractures occurred under the condition and in the position where the net-section nominal stress reached the tensile strength of the smooth specimens. First, in the specimen with a small defect (Fig. 10(a)), the net section nominal stress at the defect site is high owing to a reduction in the cross-sectional area of ≤ 3%. However, owing to the variation in tensile strength, the net section nominal stress at other areas reaches the tensile strength earlier, leading to fracture at the smooth area. Therefore, in this case, the defects are considered to have almost no effect on the tensile properties such as tensile strength and fracture strain. Next, in the specimens with medium-sized and large defects (Fig. 10(b) and (c)), the occurrence of the fractures at the defect sites is attributed to the net-section nominal stress at the defect sites reaching the tensile strength the earliest. In Region II, the stress acting on the smooth areas was higher than the 0.2% proof stress; therefore, the smooth areas exhibited plastic deformation, and the fracture strain was larger than that in Region III. In Region III, the stress acting on the smooth areas was lower than the 0.2% proof stress; therefore, the smooth areas did not exhibit plastic deformation, and the fracture strain was extremely small.

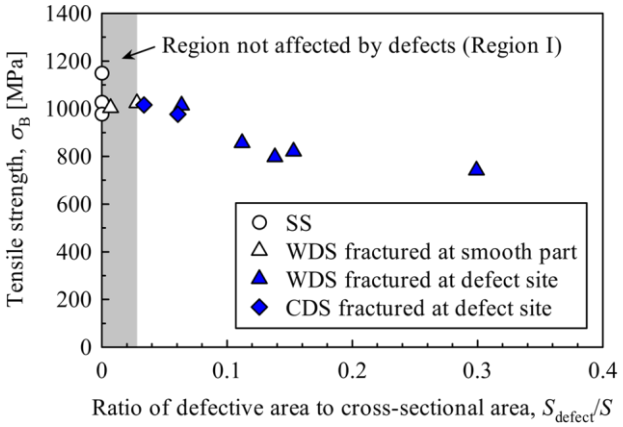

Fig. 7 Relationship between tensile strength and ratio of defective area to cross-sectional area.

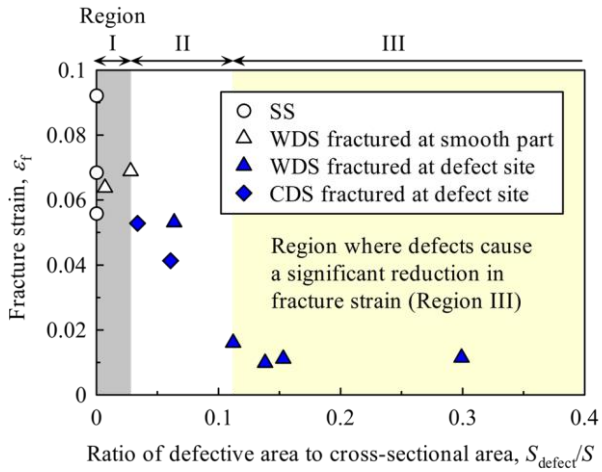

Fig. 8 Relationship between fracture strain and ratio of defective area to cross-sectional area.

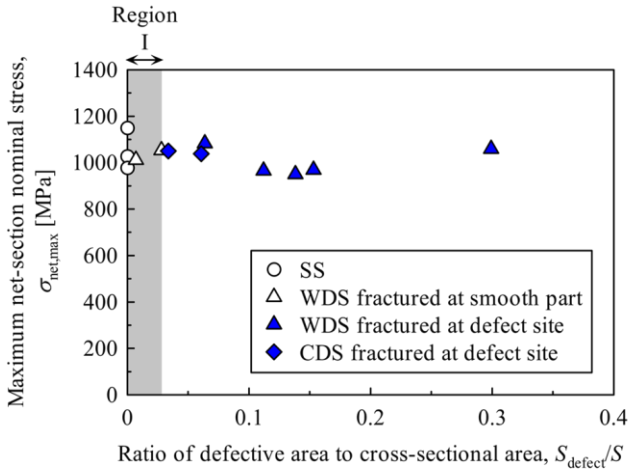

Fig. 9 Relationship between maximum net-section nominal stress and ratio of defective area to cross-sectional area.

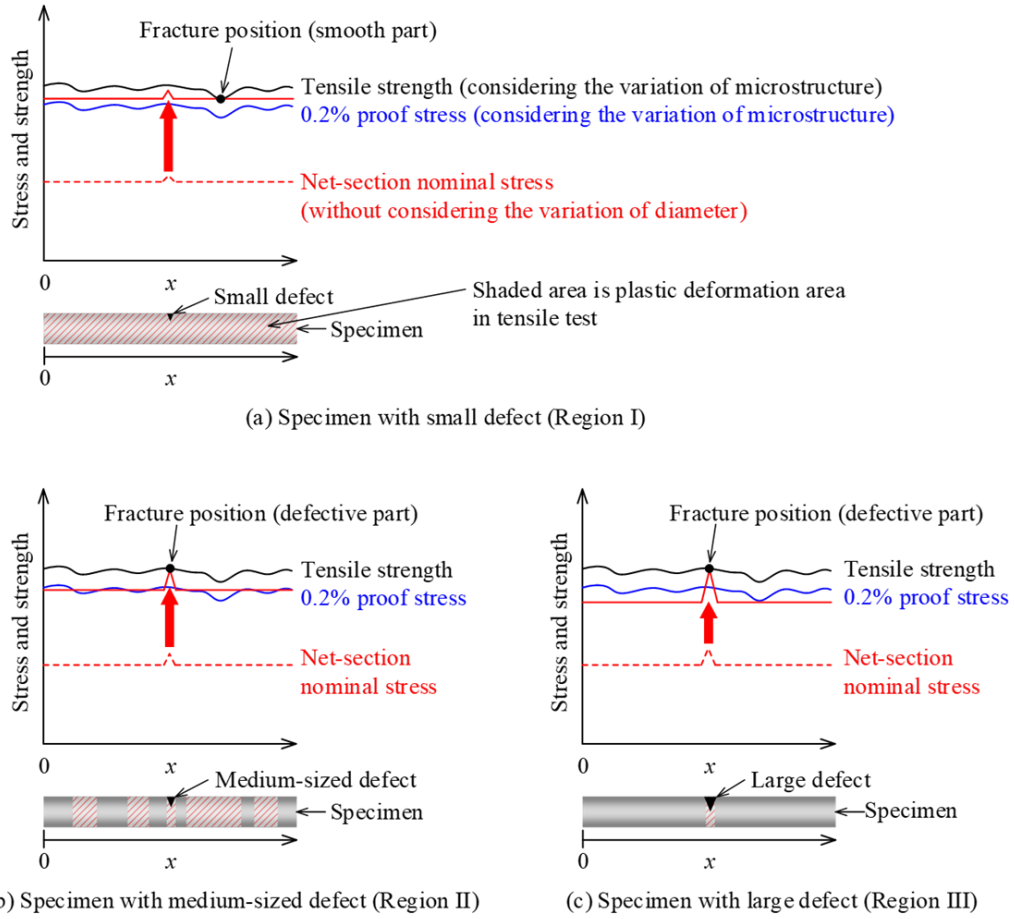

(a) Specimen with small defect (Region I)

(b) Specimen with medium-sized defect (Region II)

(c) Specimen with large defect (Region III)

Fig. 10 Schematic of distributions of tensile strength, 0.2% proof stress, and net-section nominal stress.

4. Conclusions

In this study, to investigate the effect of defects on the tensile properties of thin titanium alloy wire, tensile tests were conducted using thin Ti-6Al-4V wires in which artificial defects had been introduced via FIB processing. The results obtained were as follows:

(1) In the specimens with defects, fractures occurred when and where the net-section nominal stress reached the tensile strength of the smooth specimens. This may be due to the low notch sensitivity of titanium and the sufficient plastic deformation of the defect site, which almost eliminate the local stress concentration in the vicinity of the defect.

(2) The effect of defects on the tensile properties was classified into three regions based on the size of the defect areas. In Region I (small defect area), the specimen could fracture at either the smooth or defect site. Thus, in Region I, the defects minimally affected the tensile properties. This is attributable to variations in the cross-sectional strength of the wire. When the defect area was larger than Region I, the specimens fractured at the defect site. Thereafter, a region appeared where the fracture strain decreased gradually as the defect area (Region II) increased, and another where the fracture strain was extremely small (Region III). The boundary between Regions II and III indicates the transition from plastic deformation to no plastic deformation in the smooth area.

Acknowledgment

This study was supported by JSPS KAKENHI grant number JP21H01214 and JKA. We would like to thank Editage (www.editage.jp) for English language editing.

References

Bridier, F., Villechaise, P. and Mendez, J., Analysis of the different slip systems activated by tension in a α/β titanium

alloy in relation with local crystallographic orientation, Acta Materialia, Vol.53, No.3 (2005), pp.555-567.
Elambasseril, J., Lu, S. L., Ning, Y. P., Liu, N., Wang, J., Brandt, M., Tang, H. P. and Qian, M., 3D characterization of defects in deep-powder-bed manufactured Ti-6Al-4V and their influence on tensile properties, Materials Science & Engineering A, Vol.761 (2019), p.138031.
Horiya, T., Suzuki, H. and Kishi, T., Effect of microstructure and impurity element on fracture toughness of Ti-6Al-4V alloy, Tetsu-to-Hagane, Vol.75, No.1 (1989), pp.151-158 (in Japanese).
Miyabe, N., Tanaka, H., Nakai, Y. and Nakamura, T., Effect of yield phenomenon on fatigue damage in commercially pure iron thin wires, Transactions of the Japan Society of Mechanical Engineers Series A, Vol.77, No.784 (2011), pp.2098-2106 (in Japanese).
Narushima, T., Titanium and its alloys as biomaterials, Journal of Japan Institute of Light Metals, Vol.55, No.11 (2005), pp.561-565 (in Japanese).
Sakamoto, J., Hamada, S. and Noguchi, H., Effects of the shape of small flaws and damage due to a focused ion beam on the fatigue strength characteristics of annealed medium-carbon steel, Engineering Failure Analysis, Vol.87 (2018), pp.49-68.
Sakamoto, J., Tada, M. and Uemori, T., Tensile properties and slip deformation behavior of pure titanium thin wire with a small diameter-to-grain-size ratio, Materials Science & Engineering A, Vol.863 (2023), p.144532.
Takao, K. and Kusukawa, K., Fatigue crack initiation behavior in notched member of commercially pure titanium, Journal of the Society of Materials Science, Japan, Vol.40, No.458 (1991), pp.1422-1427 (in Japanese).
Zhang, X., Zhong, F., Shao, J., Zhang, C., Hou, N., Yuan, G. and Tu, S., Failure mechanism and mode of Ti-6Al-4V alloy under uniaxial tensile loading: Experiments and micromechanical modeling, Materials Science & Engineering A, Vol.676 (2016), pp.536-545.